

Next-Generation Multiple Access Based on NOMA with Power Level Modulation

Xinyue Pei, Yingyang Chen, Miaowen Wen, Hua Yu,

Erdal Panayirci, *Life Fellow, IEEE*, and H. Vincent Poor, *Life Fellow, IEEE*

Abstract

To cope with the explosive traffic growth of next-generation wireless communications, it is necessary to design next-generation multiple access techniques that can provide higher spectral efficiency as well as larger-scale connectivity. As a promising candidate, power-domain non-orthogonal multiple access (NOMA) has been widely studied. In conventional power-domain NOMA, multiple users are multiplexed in the same time and frequency band by different preset power levels, which, however, may limit the spectral efficiency under practical finite alphabet inputs. Inspired by the concept of spatial modulation, we propose to solve this problem by encoding extra information bits into the power levels, and exploit different signal constellations to help the receiver distinguish between them. To convey this idea, termed power selection (PS)-NOMA, clearly, we consider a simple downlink two-user NOMA system with finite input constellations. Assuming maximum-likelihood detection, we derive closed-form approximate bit error ratio (BER) expressions for both users. The achievable rates of both users are also derived in closed form. Simulation results verify the analysis and show that the proposed PS-NOMA outperforms conventional NOMA in terms of BER and achievable rate.

Index Terms

Bit error rate, next-generation multiple access (NGMA), achievable rate, finite alphabet input, non-orthogonal multiple access (NOMA).

X. Pei, M. Wen, and H. Yu are with the National Engineering Technology Research Center for Mobile Ultrasonic Detection, South China University of Technology, Guangzhou 510640, China (e-mail: eexypei@mail.scut.edu.cn; {eemwwen, yuhua}@scut.edu.cn).

Y. Chen is with Department of Electronic Engineering, College of Information Science and Technology, Jinan University, Guangzhou (e-mail: chenyy@jnu.edu.cn).

E. Panayirci is with the Department of Electrical and Electronics Engineering, Kadir Has University, 34083 Istanbul, Turkey (e-mail: eepanay@khas.edu.tr).

H. V. Poor is with the Department of Electrical and Computer Engineering, Princeton University, Princeton, NJ 08544 USA (e-mail: poor@princeton.edu).

I. INTRODUCTION

Future wireless networks, such as beyond fifth-generation (B5G) or sixth-generation (6G) networks, are expected to support extremely high data rates and numerous users or nodes with various applications and services [1]. However, the conventional orthogonal access (OMA) schemes used in the previous wireless generations cannot meet these unprecedented demands, limiting the improvement of the overall spectral efficiency (SE). Against the background, non-orthogonal multiple access (NOMA) was proposed, which allows numerous users to share the same resource (e.g., a time/frequency resource block) and separate the users in power and code domains at the expense of additional receiver complexity [2], [3]. In the power-domain NOMA, users are typically multiplexed with different power levels by using superposition coding at the transmitter and are distinguished through successive interference cancellation (SIC) at the receiver [4], [5]. Compared with OMA, NOMA has higher significant system throughput and greater fairness [6]-[8]. Due to these advantages, NOMA has been recognized as a critical technology by the third-generation partnership project (3GPP) for future wireless networks [9].

It is worth noting that the majority of existing NOMA schemes assume Gaussian input signals [10]-[12]. Although Gaussian inputs can theoretically attain the channel capacity, the corresponding implementation faces many difficulties, e.g., very large storage capacity, high computational complexity, and extremely long decoding delay [13]. Applying the results derived from the Gaussian inputs to the signals with finite alphabet inputs, e.g., pulse amplitude modulation (PAM), can result in a significant performance loss [14]. Motivated by this situation, some researchers have considered finite alphabet inputs [15]-[18]. In particular, the authors of [15] studied NOMA-aided two-user Gaussian multiple access channels (MACs) with finite complex input constellations, and the constellation-constrained capacity region of the proposed scheme was derived. Moreover, they designed a constellation rotation (CR) scheme for M -ary phase shift keying (PSK) and M -PAM signals. In [16], the same authors proposed a novel power allocation scheme for the model in [15], which can achieve similar performance as the CR scheme while reducing the decoding complexity for quadrature amplitude modulation (QAM) constellations. The authors of [17] developed a novel framework for a classical two-transmitter two-receiver NOMA system over Z -channels with QAM and max-min user fairness based on the aforementioned two studies. Specifically, they formulated a max-min optimization problem to maximize the smaller minimum Euclidean distance among the two resulting signal constellations

at both receivers. Similarly, in [18], the authors considered a classical two-user MAC with NOMA and practical QAM constellations, aiming at maximizing the minimum Euclidean distance of the received sum constellation with a maximum likelihood (ML) detector by controlling transmitted powers and phases of users.

On the other hand, spatial modulation (SM) has been regarded as another promising multi-antenna technique of improving SE for next-generation wireless networks [19]. Unlike conventional multiple-input multiple-output (MIMO), SM selects only one activated antenna for each transmission, thus avoiding inter-antenna interference and the requirement of multiple radio frequency (RF) chains. Hence, SM systems can achieve reduced implementation cost and complexity. Precisely, in SM systems, the transmitted information consists of the index of an active antenna and a modulated symbol. Clearly, combining NOMA with SM (termed SM-NOMA) will further improve system SE without increasing the power consumption and implementation complexity. Therefore, SM-NOMA has been exploited extensively in recent years, and capacity or BER performance analysis is the focus of many works [20]-[22]. In [20], an iterative algorithm for the spatial-domain design was proposed to maximize the instantaneous capacity of SM-NOMA. The authors of [21] applied SM-NOMA in wireless vehicle-to-vehicle (V2V) environments. Moreover, they analyzed closed-form capacity expressions, and BER performance via Monte Carlo simulations and formulated a pair of power allocation optimization schemes for the system. In [22], the authors studied the BER and capacity performance of a novel three-node cooperative relaying system using SM-aided NOMA. Notably, all the above mentioned works focused on Gaussian input, which do not apply to finite input constellations. Few researchers have considered finite alphabet inputs in SM-NOMA systems [23]-[26]. The authors of [23], [24] proposed and studied the respective SM-NOMA systems from their mutual information (MI) perspective. Since the MI lacks a closed-form formulation, they proposed a lower bound to quantify it. In [25], an SM aided cooperative NOMA scheme with bit allocation was studied, and its SE was analyzed. The authors of [26] mainly investigated the fundamental applicability of SM for multi-antenna channels and found intrinsic cooperation for constructing energy-efficient finite-alphabet NOMA.

However, to the best of our knowledge, all works about SM-NOMA simply considered transmitting NOMA signals in SM systems. In other words, they did not change NOMA itself. Conversely, how can we use an SM-like idea to design a novel NOMA scheme and improve its performance? Furthermore, will we be able to design the transmit power to achieve effects similar to the spatial gain in SM-NOMA? At the time of writing, no work has solved this

problem. Against the background, in this paper, we propose a novel downlink NOMA scheme using power selection (PS) with finite-alphabet inputs, termed PS-NOMA, over Rayleigh fading channels, which consists of one BS and two users. At the transmitter, except for the PAM symbols intended for the users, we also design the transmit power into the codebook, thus increasing the number of bits transmitted. The main contributions of this paper are summarized as follows:

- We design a novel PS-NOMA scheme for the classical two-user downlink channel, where the transmitter randomly chooses transmit power from the preset power matrix. Nevertheless, PS makes both transmission and decoding different from previous works. To this end, we design specific constellations and the ML detector for the proposed scheme. We further discuss the influence caused by different configurations of the power matrix and give the optimal order of the matrix. Moreover, we calculate the best design for the power matrix based on the minimum Euclidean distance of the constellation.
- The performance of PS-NOMA is theoretically analyzed in terms of BER and achievable rate. We derive closed-form achievable rate expressions for PS-NOMA. Since it is difficult to derive exact BER expressions, approximate closed-form BER expressions are derived for users employing M -ary PAM instead, which well match with the simulation counterparts. It is worth noting that all derived results are restricted to specific constellations and Rayleigh fading channels.
- Monte Carlo simulations are performed to verify the theoretical analysis. In consideration of fairness, conventional NOMA without PS (termed NOMA) is used as a benchmark. Simulation results show that PS-NOMA outperforms NOMA in terms of BER and achievable rate.

The rest of this paper is organized as follows. Section II describes the system model of PS-NOMA. Section III provides the achievable rate and BER analyses. Section IV analyzes the numerical results. Finally, we conclude the work in Section V.

Notation: The probability of an event and the probability density function (PDF) of a random variable are denoted by $\Pr(\cdot)$ and $p(\cdot)$, respectively. $Q(\cdot)$, $\Gamma(\cdot)$, $\mathbb{E}\{\cdot\}$, and $\text{Var}\{\cdot\}$ denote the Gaussian Q-function, gamma function, expectation, and variance, respectively. $|\cdot|$ denotes the absolute value of a complex scalar. $\lfloor \cdot \rfloor$ denotes the floor function. $\mathcal{R}\{\cdot\}$ indicates the real part of a complex value. Superscript $*$ stands for complex conjugates. $I(\cdot)$ denotes MI, and $H(\cdot|\cdot)$ denotes entropy. Finally, $x \sim \mathcal{N}_c(\mu_x, \beta_x)$ indicates that the random variable x obeys a complex

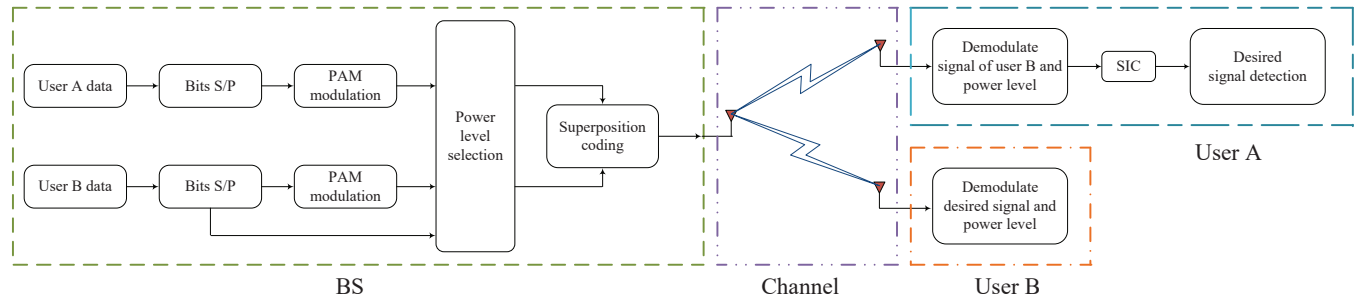


Fig. 1. System model with 2 users and $N = 2$.

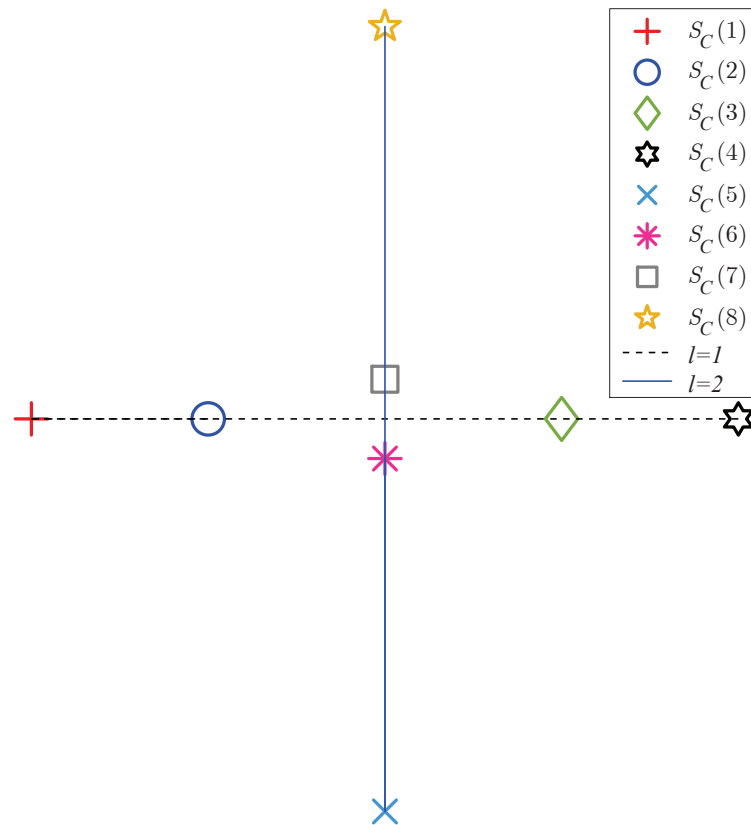


Fig. 2. Constellation $S_C(i)$ ($i \in \{1, \dots, 8\}$) of superimposed signal transmitted with 2-PAM signals s_A as well as s_B and $N = 2$.

Gaussian distribution with mean μ_x and variance β_x .

II. SYSTEM MODEL

A. Transmission Model

Before introducing PS-NOMA, let us recall the conventional downlink two-user NOMA system first. In such a system, the base station (denoted by BS) transmits a superimposed signal to the users. Based on the NOMA protocol, this signal consists of the data symbols desired by both users, and the power allocated to the symbols. In conventional NOMA systems, information is carried out only by data symbols. However, the power allocation coefficients contained in the superimposed signal can also be utilized to carry information by appropriate design.

Based on this idea, we consider a downlink PS-NOMA network as illustrated in Fig. 1, which consists of a BS, a near user (denoted by U_A), a far user (denoted by U_B). All the nodes are equipped with a single antenna. The channels of $BS \rightarrow U_A$ and $BS \rightarrow U_B$ are respectively denoted by h_A and h_B , which are assumed to follow $\mathcal{N}_c(0, \beta_A)$ and $\mathcal{N}_c(0, \beta_B)$ distributions. Notably, in our system, all the nodes are assumed to be synchronous in both time and frequency. Moreover, complete and perfect channel state information (CSI) is assumed to be available to users. Unlike conventional NOMA, we obtain a spectral efficiency gain by selecting a power level (PL) at the transmitter. Similar to the SM, a PL is chosen from a set of PLs N at random where $N = 2^k$, $k = 1, 2, \dots$, so that each PL carries $\log_2(N)$ bits of information in addition to the amount of information carried by the transmitted data symbols. Noticing that U_A is the near user and U_B is the far user, we have $\beta_A \geq \beta_B$, and the power allocated to U_A should be smaller than that assigned to U_B according to the principle of NOMA [4]. In this manner, the transmit power allocation coefficient matrix can be written as

$$\mathbf{P} = \begin{bmatrix} \sqrt{p_A(1)}, & \sqrt{1 - p_A(1)} \\ \sqrt{p_A(2)}, & \sqrt{1 - p_A(2)} \\ \dots & \dots \\ \sqrt{p_A(N)}, & \sqrt{1 - p_A(N)} \end{bmatrix}, \quad (1)$$

where the first ($0 < p_A(l) < 0.5$, $l \in \{1, \dots, N\}$) and the second columns represent the power allocation coefficient for U_A and U_B , respectively, and different rows represent different PLs. To ensure the PLs are distinguishable, we deliberately rotate each PL with a certain angle, which is given by $\Theta = \text{diag}(\exp(0), \exp(j\pi/N), \dots, \exp(j(N-1)\pi/N))$. Therefore, the rotated power

allocation coefficient matrix can be derived as

$$\mathbf{G} = \mathbf{\Theta}\mathbf{P} = \begin{bmatrix} \alpha_A(1), & \alpha_B(1) \\ \alpha_A(2), & \alpha_B(2) \\ \dots & \dots \\ \alpha_A(N), & \alpha_B(N) \end{bmatrix}, \quad (2)$$

where $\alpha_A(l) = \exp(j(l-1)\pi/N)p_A(l)$ and $\alpha_B(l) = \exp(j(l-1)\pi/N)(1-p_A(l))$.

During each transmission, the BS first chooses the PL $l \in \mathcal{N}$ ($\mathcal{N} = 1, 2, \dots, N$) as the transmit power. Subsequently, it conveys the superposition coded symbol

$$s_C = \alpha_A(l)s_A + \alpha_B(l)s_B \quad (3)$$

to U_A and U_B simultaneously, where $s_A \in \mathcal{S}_A$ and $s_B \in \mathcal{S}_B$ are the data symbols intended for U_A and U_B , respectively. We assume that s_A and s_B are M_A -ary PAM and M_B -ary PAM symbols with $\mathbb{E}\{|s_A|^2\} = \mathbb{E}\{|s_B|^2\} = 1$;

$$\mathcal{S}_A = \{\pm d_A, \pm 3d_A, \dots, \pm(2M_A - 1)d_A\} \quad (4)$$

and

$$\mathcal{S}_B = \{\pm d_B, \pm 3d_B, \dots, \pm(2M_B - 1)d_B\} \quad (5)$$

are the corresponding M_A and M_B points constellations, respectively, where $d_A = \sqrt{3/(M_A^2 - 1)}$ and $d_B = \sqrt{3/(M_B^2 - 1)}$ respectively represent half of the minimum distance between two adjacent points of the normalized M_A -PAM and M_B -PAM constellations. Let $\mathcal{M}_i = \{1, 2, \dots, M_i\}$ ($i \in \{A, B\}$), the signal constellation of s_C can be expressed as

$$\mathcal{S}_C = \{s_C | s_i = \mathcal{S}_i(k_i), \text{PL} = l, k_i \in \mathcal{M}_i, l \in \mathcal{N}, i \in \{A, B\}\}, \quad (6)$$

which is an irregular $M_A M_B N$ -ary constellation, as shown in Fig. 2. Consequently, the received signals at U_A and U_B can be given by

$$y_A = h_A s_C + n_A \quad (7)$$

and

$$y_B = h_B s_C + n_B, \quad (8)$$

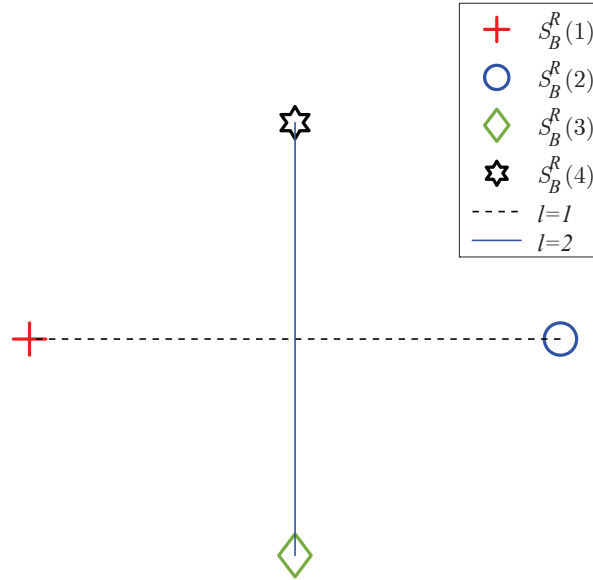


Fig. 3. Constellations of s_B with $N = 2$, where s_B is a 2-PAM symbol, and \mathcal{S}_B^R denotes the union constellation of s_B and PL. $\mathcal{S}_B^R(1), \mathcal{S}_B^R(3) : s_B = -1$, $\mathcal{S}_B^R(2), \mathcal{S}_B^R(4) : s_B = 1$.

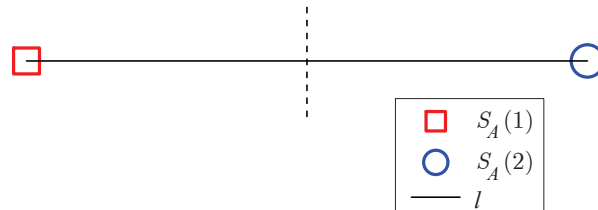


Fig. 4. Constellation of 2-PAM signal s_A .

respectively, where $n_A \sim \mathcal{N}_c(0, N_0)$ ($n_B \sim \mathcal{N}_c(0, N_0)$) indicates the additive white Gaussian noise (AWGN) at U_A (U_B) with power spectral density N_0 .

B. Signal Decoding

The above subsection describes the transmission model of PS-NOMA. Now we shift our focus to the decoding process. Before the following description, we need to first clarify which data symbol gets the information of the PL. *In this paper, we use the information of PL to enhance*

Algorithm 1 Detection Algorithm1: **for** U_A **do**2: Compare the received signal y_A with the joint constellation \mathcal{S}_B^R :

$$\mathcal{S}_B^R(\hat{i}) = \arg \min_i |y_A - h_A \mathcal{S}_B^R(i)|^2, \quad (9)$$

where $i \in \{1, \dots, NM_B\}$, and \hat{i} is the estimate of i at U_A .3: Determine active PL \hat{l} and the transmitted signal \hat{s}_B by resolving $\mathcal{S}_B^R(\hat{i})$, where \hat{s}_B and \hat{l} are the estimates of s_B and l at U_A .4: Use SIC to decode s_A , whose ML detector can be expressed as

$$\hat{s}_A = \arg \min_{s_A} |y_A - h_A \alpha_B(\hat{l}) \hat{s}_B - h_A \alpha_A(\hat{l}) s_A|^2, \quad (10)$$

where \hat{s}_A is the estimate of s_A at U_A .5: **end for**6: **for** U_B **do**7: Compare the received signal y_B with the joint constellation \mathcal{S}_B^R :

$$\mathcal{S}_B^R(\hat{i}) = \arg \min_i |y_B - h_A \mathcal{S}_B^R(i)|^2, \quad (11)$$

where $i \in \{1, \dots, NM_B\}$, and \hat{i} is the estimate of i at U_B .8: Determine active PL \hat{l} and the transmitted signal \hat{s}_B by resolving $\mathcal{S}_B^R(\hat{i})$, where \hat{s}_B and \hat{l} are the estimates of s_B and l at U_B .9: **end for**

the performance of U_B . In other scenarios, it can also be used to improve the performance of U_A .

It is assumed that both users invoke ML detectors to decode their signals. As we know, PL is an important factor affecting the decoding procedure because it is closely related to SIC and the decoding of data symbols. In conventional NOMA scheme, whose PLs are fixed, the users already know the values of PLs when decoding. While in PS-NOMA, PLs change over time and are unknown at the users. Hence, the conventional ML detector cannot be applied directly in PS-NOMA, and we should also decode PL at both users. Under the NOMA protocol, U_A first decodes s_B and l ; for U_B , it detects s_B and l by treating s_A as noise. We herein use the joint constellation of s_B and PL to help decoding. For example, in the case of $N = 2$ and 2-PAM s_B as shown in Fig. 3, a combined 4-ary constellation is formed with four points, i.e.,

$$\mathcal{S}_B^R(i) = \{s_B = \pm 1, l = 1, 2\}, i \in \{1, \dots, 4\}. \quad (12)$$

Explicitly, the information of s_B and PL is contained in each point of the constellation. If the received signal after equalization is close to $\mathcal{S}_B^R(1)$, we can readily know the estimated $s_B = -1$ and $l = 1$. With these information, U_A then subtracts the estimated s_B and decodes its own

signal, and this procedure can be seen as a common 2-PAM signal decoding as shown in Fig. 4. The detailed detection algorithm for both users are summarized in **Algorithm 1**.

III. PERFORMANCE ANALYSIS

In this section, we theoretically analyze the performance of the proposed PS-NOMA scheme in terms of achievable rate and BER. Moreover, we discuss the optimal design of N and \mathbf{G} .

A. Achievable Rate Analysis

For convenience, we let $\{a, b, l\}$ ($a \in \mathcal{M}_A$, $b \in \mathcal{M}_B$, $l \in \mathcal{N}$) denote $(\alpha_A(l)\mathcal{S}_A(a) + \alpha_B(l)\mathcal{S}_B(b))$. It is considered that all PLs are activated equally likely for PS-NOMA.

1) *Achievable Rate Analysis of U_B* : It follows from the chain rule that

$$I(s_B, \text{PL}; y_B) = I(s_B; y_B | \text{PL}) + I(\text{PL}; y_B). \quad (13)$$

Therefore, we deal with the calculations of $I(s_B; y_B | \text{PL})$ and $I(\text{PL}; y_B)$ in the following. Specifically, we have

$$I(s_B; y_B | \text{PL}) = H(y_B | \text{PL}) - H(y_B | s_B, \text{PL}), \quad (14)$$

where

$$H(y_B | \text{PL}) = \frac{1}{N} \sum_{l=1}^N H(y_B | \text{PL} = l) \quad (15)$$

and

$$H(y_B | s_B, \text{PL}) = \frac{1}{NM_B} \sum_{k_B=1}^{M_B} \sum_{l=1}^N H(y_B | s_B = \mathcal{S}_B(k_B), \text{PL} = l). \quad (16)$$

Here, $H(y_B | \text{PL} = l)$ and $H(y_B | s_B = \mathcal{S}_B(k_B), \text{PL} = l)$ can be respectively given by

$$\begin{aligned} H(y_B | \text{PL} = l) &= \int p(y_B | \text{PL} = l) \log_2(p(y_B | \text{PL} = l)) dy_B \\ &= - \frac{\sum_{k_A=1}^{M_A} \sum_{k_B=1}^{M_B} \sum_{l=1}^N \log_2 \left(\sum_{i_A=1}^{M_A} \sum_{i_B=1}^{M_B} p(y_B | s_A = \mathcal{S}_A(i_A), s_B = \mathcal{S}_B(i_B), \text{PL} = l) / M_A M_B \right)}{M_A M_B N} \end{aligned} \quad (17)$$

and

$$\begin{aligned} H(y_B|s_B = \mathcal{S}_B(k_B), \text{PL} = l) &= \int p(y_B|s_B = \mathcal{S}_B(k_B), \text{PL} = l) \log_2(p(y_B|s_B = \mathcal{S}_B(k_B), \text{PL} = l)) dy_B \\ &= - \frac{\sum_{k_A=1}^{M_A} \sum_{k_B=1}^{M_B} \sum_{l=1}^N \log_2 \left(\sum_{i_A=1}^{M_A} p(y_B|s_A = \mathcal{S}_A(i_A), s_B = \mathcal{S}_B(k_B), \text{PL} = l) / M_A \right)}{M_A M_B N}. \end{aligned} \quad (18)$$

Substituting (17), (18), and

$$p(y_B|s_A = \mathcal{S}_A(i_A), s_B = \mathcal{S}_B(i_B), \text{PL} = l) = \frac{1}{\pi N_0} \exp \left(-\frac{|y_B - h_B\{i_A, i_B, l\}|^2}{N_0} \right) \quad (19)$$

into (14), $I(s_B; y_B|\text{PL})$ can be given by

$$\begin{aligned} I(s_B; y_B|\text{PL}) &= \log_2(M_B) - \frac{1}{M_A M_B N} \\ &\times \sum_{k_A=1}^{M_A} \sum_{k_B=1}^{M_B} \sum_{l=1}^N \mathbb{E} \left\{ \log_2 \left(\frac{\sum_{i_A=1}^{M_A} \sum_{i_B=1}^{M_B} \exp(-|h_B\{k_A, k_B, l\} - h_B\{i_A, i_B, l\} + n_B|^2/N_0)}{\sum_{i_A=1}^{M_A} \exp(-|h_B\{k_A, k_B, l\} - h_B\{i_A, k_B, l\} + n_B|^2/N_0)} \right) \right\}. \end{aligned} \quad (20)$$

In this manner, $I(\text{PL}; y_B)$ can also be derived as

$$\begin{aligned} I(\text{PL}; y_B) &= H(y_B) - H(y_B|\text{PL}) \\ &= \log_2(N) + \frac{1}{M_A M_B N} \\ &\times \sum_{k_A=1}^{M_A} \sum_{k_B=1}^{M_B} \sum_{l=1}^N \mathbb{E} \left\{ \log_2 \left(\frac{\sum_{i_A=1}^{M_A} \sum_{i_B=1}^{M_B} \exp(-|h_B\{k_A, k_B, l\} - h_B\{i_A, i_B, l\} + n_B|^2/N_0)}{\sum_{i_A=1}^{M_A} \sum_{i_B=1}^{M_B} \sum_{ll=1}^N \exp(-|h_B\{k_A, k_B, l\} - h_B\{i_A, i_B, ll\} + n_B|^2/N_0)} \right) \right\}. \end{aligned} \quad (21)$$

2) *Achievable Rate Analysis of U_A* : Different from U_B , U_A detects its own signal after removing the interference imposed by U_B . By invoking a similar mathematical method, the achievable rate for U_A detecting s_B is given by

$$I(s_B, \text{PL}; y_A) = I(s_B; y_A|\text{PL}) + I(\text{PL}; y_A), \quad (22)$$

where $I(s_B; y_A|\text{PL})$ and $I(\text{PL}; y_A)$ can be respectively derived as

$$I(s_B; y_A|\text{PL}) = \log_2(M_B) - \frac{1}{M_A M_B N}$$

$$\times \sum_{k_A=1}^{M_A} \sum_{k_B=1}^{M_B} \sum_{l=1}^N \mathbb{E} \left\{ \log_2 \left(\frac{\sum_{i_A=1}^{M_A} \sum_{i_B=1}^{M_B} \exp(-|h_A\{k_A, k_B, l\} - h_A\{i_A, i_B, l\} + n_A|^2/N_0)}{\sum_{i_A=1}^{M_A} \exp(-|h_A\{k_A, k_B, l\} - h_A\{i_A, k_B, l\} + n_A|^2/N_0)} \right) \right\} \quad (23)$$

and

$$I(\text{PL}; y_A) = \log_2(N) + \frac{1}{M_A M_B N} \times \sum_{k_A=1}^{M_A} \sum_{k_B=1}^{M_B} \sum_{l=1}^N \mathbb{E} \left\{ \log_2 \left(\frac{\sum_{i_A=1}^{M_A} \sum_{i_B=1}^{M_B} \exp(-|h_A\{k_A, k_B, l\} - h_A\{i_A, i_B, l\} + n_A|^2/N_0)}{\sum_{i_A=1}^{M_A} \sum_{i_B=1}^{M_B} \sum_{ll=1}^N \exp(-|h_A\{k_A, k_B, l\} - h_A\{i_A, i_B, ll\} + n_A|^2/N_0)} \right) \right\}. \quad (24)$$

With the detected PL, the achievable rate for U_A detecting s_A , i.e., $I(s_A; y_A|\text{PL})$ can be derived as

$$I(s_A; y_A|\text{PL}) = \log_2(M_A) - \frac{1}{M_A N} \times \sum_{k_A=1}^{M_A} \sum_{l=1}^N \mathbb{E} \left\{ \log_2 \left(\frac{\sum_{i_A=1}^{M_A} \exp(|h_A \alpha_A(l)(\mathcal{S}_A(k_A) - \mathcal{S}_A(i_A)) + n_A|^2/N_0)}{\exp(-|n_A|^2/N_0)} \right) \right\}. \quad (25)$$

B. BER Analysis

In this subsection, closed-form BER expressions are derived for U_A and U_B in PS-NOMA systems.

1) *BER of U_B* : To obtain the BER of U_B , we should derive the symbol error ratio (SER) of s_B at U_B first. Similar to [27], [28], we utilize the conditional pairwise error probability (PEP), which indicates the probability of detecting s_B as \hat{s}_B conditioned on h_B , namely

$$\begin{aligned} & \Pr(s_B \rightarrow \hat{s}_B | h_B) \\ &= \Pr(|y_B - h_B \alpha_B(l) s_B|^2 > |y_B - h_B \alpha_B(\hat{l}) \hat{s}_B|^2) \\ &\stackrel{(a)}{=} \Pr(|h_B x_B|^2 - |h_B \hat{x}_B|^2 - 2\mathcal{R}\{y_B^* h_B (x_B - \hat{x}_B)\} > 0) \\ &\stackrel{(b)}{=} \Pr(-|h_B \Delta x_B|^2 - 2\mathcal{R}\{w_B^* h_B \Delta x_B\} > 0) \\ &\stackrel{(c)}{=} Q \left(\sqrt{\frac{|h_B|^2 (|\Delta x_B|^2 + 2\mathcal{R}\{x_A^* \Delta x_B\})^2}{2N_0 |\Delta x_B|^2}} \right) \\ &\stackrel{(d)}{=} Q \left(\sqrt{\frac{|h_B|^2}{2N_0^{\text{equal}}}} \right), \end{aligned} \quad (26)$$

where we define in (a) $x_B \triangleq \alpha_B(l)s_B$ and $\hat{x}_B \triangleq \alpha_B(\hat{l})\hat{s}_B$; in (b) $w_B = h_B\alpha_A(l)s_A + n_B = h_Bx_A + n_B$, with $x_A \triangleq \alpha_A(l)s_A$, and $\Delta x_B = x_B - \hat{x}_B$; the detailed derivation of (c) is present in Appendix A; (d) is obtained by defining equivalent noise variance as

$$N_0^{\text{equal}} \triangleq \frac{N_0|\Delta x_B|^2}{(|\Delta x_B|^2 + 2\mathcal{R}\{x_A^*\Delta x_B\})^2}. \quad (27)$$

Since we model h_B as a complex Gaussian random variable, $|h_B|^2$ has a PDF

$$p_{|h_B|^2}(x) = \frac{1}{\beta_B} \exp\left(-\frac{x}{\beta_B}\right). \quad (28)$$

With $p_{|h_B|^2}(x)$, we can arrive at [29, Eq. (64)]

$$\begin{aligned} \Pr(s_B \rightarrow \hat{s}_B) &= \int_0^{+\infty} \Pr(s_B \rightarrow \hat{s}_B|h_B)p_{|h_B|^2}(x)dx \\ &= \int_0^{+\infty} Q\left(\sqrt{\frac{|h_B|^2}{2N_0^{\text{equal}}}}\right)p_{|h_B|^2}(x)dx \\ &= \frac{1}{2} \left(1 - \sqrt{\frac{\beta_B}{4N_0^{\text{equal}} + \beta_B}}\right), \end{aligned} \quad (29)$$

which can be averaged over all the possible values of x_A^* to consider all interference scenarios. Notably, x_A herein should keep the same PL as x_B . Let $P_{ij,B}^{\text{bit}}$ denote the number of error bits when symbol $\mathcal{S}_B^R(i)$ is incorrectly detected as $\mathcal{S}_B^R(j)$. Since s_B and PL have $\log_2(NM_B)$ bits, the BER of s_B and PL detections at U_B can be approximated by

$$P_B \approx \frac{1}{NM_B \log_2(NM_B)} \sum_{i=1}^{NM_B} \sum_{j \neq i} \Pr(\mathcal{S}_B^R(i) \rightarrow \mathcal{S}_B^R(j))P_{ij,B}^{\text{bit}}. \quad (30)$$

2) *BER of U_A* : Recall the ML detection in (9) and (10). U_A first decodes PL as well as s_B and extracts s_B from the received signal y_A and then decodes s_A from the residual signal. Obviously, the overall BER can be divided into two complementary parts, depending on whether s_B and PL $l \in \mathcal{N}$ are correctly detected or not. Since we have N PLs, the overall BER of U_A can be evaluated as

$$P_A \approx (1 - P_A^{s_B}) \left(\frac{1}{N} \sum_{l=1}^N P_{\text{bit}}^A(l) \right) + \frac{P_A^{s_B}}{2}, \quad (31)$$

where $P_A^{s_B}$ is the SER of s_B at U_A , and $P_{\text{bit}}^A(l)$ denotes the BER of M_A -ary PAM demodulation over Rayleigh fading channels with PL l selected. Since it is difficult to exactly calculate the

BER when s_B or PL is detected incorrectly at U_A , we use the estimate $P_A^{sB}/2$ instead. Similarly, to derive P_A^{sB} , we use the conditional PEP, which denotes the probability of detecting s_B as \hat{s}_B conditioned on h_A [27], [28]

$$\begin{aligned}
& \Pr(s_B \rightarrow \hat{s}_B | h_A) \\
&= \Pr(|y_A - h_A \alpha_B(l) s_B|^2 > |y_A - h_A \alpha_B(\hat{l}) \hat{s}_B|^2) \\
&= Q \left(\sqrt{\frac{|h_A|^2 (|\Delta x_B|^2 + 2\mathcal{R}\{x_A^* \Delta x_B\})^2}{2N_0 |\Delta x_B|^2}} \right) \\
&= Q \left(\sqrt{\frac{|h_A|^2}{2N_0^{\text{equal}}}} \right). \tag{32}
\end{aligned}$$

Definitions of x_B , \hat{x}_B , x_A , Δx_B , and N_0^{equal} are given in (26) and (27). Having

$$p_{|h_A|^2}(x) = \frac{1}{\beta_A} \exp\left(-\frac{x}{\beta_A}\right), \tag{33}$$

we can arrive at [29, Eq. (64)]

$$\begin{aligned}
\Pr(s_B \rightarrow \hat{s}_B) &= \int_0^{+\infty} \Pr(s_B \rightarrow \hat{s}_B | h_A) p_{|h_A|^2}(x) dx \\
&= \frac{1}{2} \left(1 - \sqrt{\frac{\beta_A}{4N_0 + \beta_A}} \right), \tag{34}
\end{aligned}$$

which can be averaged over all the possible values of x_A^* to consider all interference scenarios.

Equally, the x_A herein should keep the same PL as x_B . Hence, P_A^{sB} is given by

$$P_A^{sB} \approx \frac{1}{NM_B} \sum_{i=1}^{NM_B} \sum_{j \neq i} \Pr(\mathcal{S}_B^R(i) \rightarrow \mathcal{S}_B^R(j)). \tag{35}$$

As for the calculation of $P_{\text{bit}}^A(l)$, we first derive the conditional error probability for PL l under the m_A -th bit ($m_A \in \{1, \dots, \log_2(M_A)\}$) and the conditions of receive signal-to-noise ratio (SNR) at U_A , i.e.,

$$\gamma_A = \frac{\alpha_A(l)^2 |h_A|^2}{N_0}, \tag{36}$$

as [30]

$$P_{\text{bit}}^A(l | m_A, \gamma_A) = \frac{2}{M_A}$$

$$\times \sum_{i=0}^{(1-2^{-m_A})M_A-1} \left\{ (-1)^{\lfloor i(2^{m_A}-1)/M_A \rfloor} \left(2^{m_A-1} - \lfloor \frac{i(2^{m_A}-1)}{M} + \frac{1}{2} \rfloor \right) Q \left((2i+1)d_A \sqrt{2\gamma_A} \right) \right\}. \quad (37)$$

By substituting the alternative representation, i.e.,

$$Q(x) = \frac{1}{\pi} \int_0^{\frac{\pi}{2}} \exp \left(-\frac{x^2}{2 \sin^2 \psi} \right) d\psi \quad (38)$$

for the Gaussian Q-function in (37), we can obtain

$$\begin{aligned} P_{\text{bit}}^A(l|m_A, \gamma_A) &= \frac{2}{M_A} \sum_{i=0}^{(1-2^{-m_A})M_A-1} \left\{ (-1)^{\lfloor \frac{i(2^{m_A}-1)}{M_A} \rfloor} \right. \\ &\quad \times \left(2^{m_A-1} - \lfloor \frac{i(2^{m_A}-1)}{M} + \frac{1}{2} \rfloor \right) \\ &\quad \times \underbrace{\frac{1}{\pi} \int_0^{\pi/2} \exp \left(-\frac{((2i+1)d_A)^2 \gamma_A}{\sin^2 \psi} \right) d\psi}_{\mathcal{Q}(i|\gamma_A)} \left. \right\}. \end{aligned} \quad (39)$$

By statistically averaging the equation above over the PDF of γ_A , which is given by

$$p_{\gamma_A}(\gamma_A) = \frac{N_0}{(\alpha_A(l))^2 \beta_A} \exp \left(\frac{-N_0 \gamma_A}{(\alpha_A(l))^2 \beta_A} \right), \quad (40)$$

$\mathcal{Q}(i)$ can be derived as

$$\mathcal{Q}(i) = \frac{1}{\pi} \int_0^{\frac{\pi}{2}} \int_0^{\infty} \exp \left(-\frac{((2i+1)d_A)^2 \gamma_A}{\sin^2 \psi} \right) p_{\gamma_A}(\gamma_A) d\gamma_A d\psi = \frac{1 - \mathcal{G}(i)}{2}, \quad (41)$$

where

$$\mathcal{G}(i) = \sqrt{\frac{(\alpha_A(l))^2 \beta_A ((2i+1)d_A)^2}{N_0 + (\alpha_A(l))^2 \beta_A ((2i+1)d_A)^2}}. \quad (42)$$

In this manner, we have

$$P_{\text{bit}}^A(l|m_A) = \frac{2}{M_A} \sum_{i=0}^{(1-2^{-m_A})M_A-1} \left\{ (-1)^{\lfloor \frac{i(2^{m_A}-1)}{M_A} \rfloor} \left(2^{m_A-1} - \lfloor \frac{i(2^{m_A}-1)}{M} + \frac{1}{2} \rfloor \right) \mathcal{Q}(i) \right\}. \quad (43)$$

Therefore, we have

$$P_{\text{bit}}^A(l) = \frac{1}{\log_2(M_A)} \sum_{m_A=1}^{\log_2(M_A)} P_{\text{bit}}^A(l|m_A). \quad (44)$$

Finally, by substituting (35) and (44) into (31), we can derive the expression of P_A .

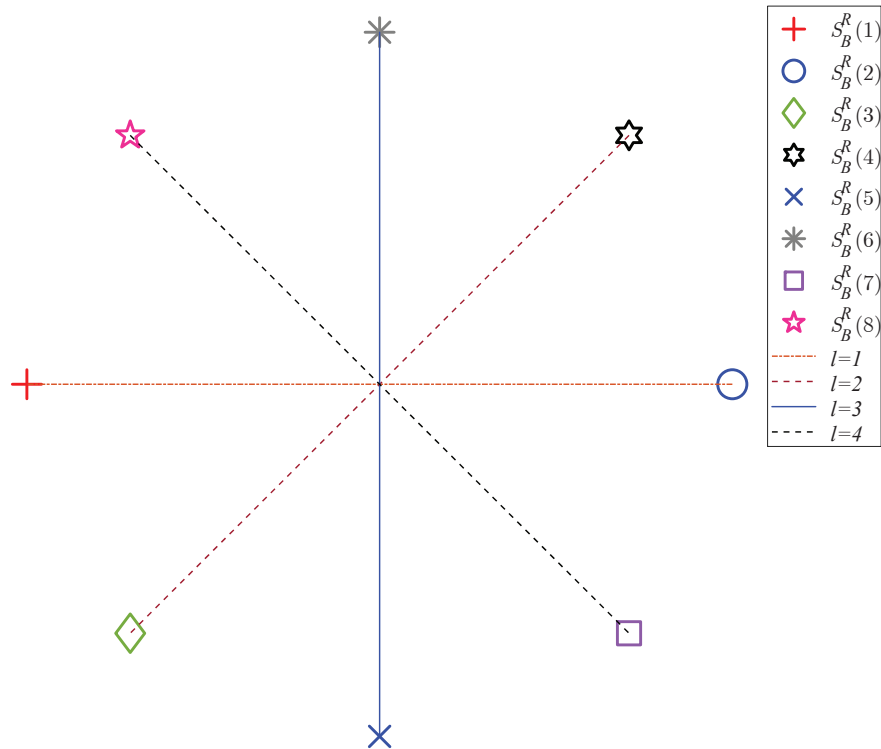


Fig. 5. Constellations of s_B with $N = 4$, where s_B is a 2-PAM symbol, and \mathcal{S}_B^R denotes the union constellation of s_B and PL.

C. Optimal Constellation Analysis

In this subsection, we discuss the optimal design of constellation in terms of the values of N as well as \mathbf{G} . For convenience, let $d_{B,ij}$ denote the Euclidean distance between points $\mathcal{S}_B^R(i)$ and $\mathcal{S}_B^R(j)$, where $i, j \in \{1, \dots, NM_B\}$. According to the geometric analysis, we can obtain the following.

Lemma 1. *Optimal BER performance is achieved at $N = 2$.*

Proof. Since the cases of $N \geq 2$ all have similar derivation processes, we can obtain pattern by analyzing a certain case. For ease of discussion, we consider the 2-PAM signal s_A , 2-PAM signal s_B , and $N = 4$ scenario as an example. As indicated in **Algorithm 1**, N only affects the order of combined constellation. When $N = 4$, the combined constellation is shown as Fig. 5. Let $d_{B,i,\min}$ denotes the minimum Euclidean distance between $\mathcal{S}_B^R(i)$ and other points. Considering the symmetry of Fig. 5, we first take $\mathcal{S}_B^R(1)$ for instance. From Fig. 5, we can obtain $d_{B,1,\min}$ as

$$d_{B,1,\min} = \min\{d_{B,12}, d_{B,13}, d_{B,16}, d_{B,18}\}, \quad (45)$$

where

$$d_{B,12} = 2d_B|\alpha_B(1)|, \quad (46)$$

$$d_{B,13} = \sqrt{|d_B\alpha_B(1)|^2 + |d_B\alpha_B(2)|^2 - 2d_B^2|\alpha_B(1)\alpha_B(2)|\cos\left(\frac{\pi}{N}\right)}, \quad (47)$$

$$d_{B,16} = \sqrt{|d_B\alpha_B(1)|^2 + |d_B\alpha_B(3)|^2 - 2d_B^2|\alpha_B(1)\alpha_B(3)|\cos\left(\frac{2\pi}{N}\right)}, \quad (48)$$

and

$$d_{B,18} = \sqrt{|d_B\alpha_B(1)|^2 + |d_B\alpha_B(4)|^2 - 2d_B^2|\alpha_B(1)\alpha_B(4)|\cos\left(\frac{\pi}{N}\right)}, \quad (49)$$

respectively. In the similar manner, we can derive $d_{B,2,\min}$, and so on. Therefore, the minimum Euclidean distance of Fig. 5, can be derived as

$$d_{B,\min} = \min\{d_{B,1,\min}, d_{B,2,\min}, d_{B,3,\min}, d_{B,4,\min}, d_{B,5,\min}, d_{B,6,\min}, d_{B,7,\min}, d_{B,8,\min}\}. \quad (50)$$

Since we have $N \geq 2$, the angle π/N and $2\pi/N$ are values between 0 and π . In other words, $\cos(\pi/N)$ is monotonously increasing with respect to N . Evidently, to achieve optimal BER performance, N should be equal to the minimum value, which proves **Lemma 1**. \square

Corollary 1. *Optimal BER performance is achievable when the information of PL is only carried out by the difference of angle.*

Proof. According to **Lemma 1**, we consider 2-PAM signal s_A , 2-PAM signal s_B , and $N = 2$ scenario in the following. Unlike the derivation of **Lemma 1**, here we should also consider the BER performance of U_A . We begin with the analysis of s_A , whose constellation is Fig. 4. In this manner, its minimum Euclidean distance can be derived as

$$d_{A,\min} = 2d_A|\alpha_A(l)|, \quad (51)$$

where $l \in \mathcal{N}$. Obviously, $d_{A,\min}$ is determined by the minimum value of $|\alpha_A(l)|$. Therefore, if $|\alpha_A(l)|$ with different l has a constant value, $d_{A,\min}$ will be optimal and easy to design. For example, if we consider the case where $|\alpha_A(1)| = 0.2$, $|\alpha_A(2)| = 0.1$, and the case where $|\alpha_A(1)| = |\alpha_A(2)| = 0.2$. It is clear that the latter case has larger $d_{A,\min}$. Then we shift our focus

to s_B . The combined constellation is shown as Fig. 3, whose minimum Euclidean distance can be written as

$$d_{B,\min} = \min\{d_{B,12}, d_{B,34}, d_{B,14}, d_{B,23}\}, \quad (52)$$

where

$$d_{B,12} = 2d_B|\alpha_B(1)|, \quad (53)$$

$$d_{B,34} = 2d_B|\alpha_B(2)|, \quad (54)$$

and

$$d_{B,14} = d_{B,23} = \sqrt{|d_B\alpha_B(1)|^2 + |d_B\alpha_B(2)|^2}. \quad (55)$$

Collating (55) with (53) and (54), it is clear that $d_{B,\min}$ is determined by the minimum value of $|\alpha_B(1)|$ and $|\alpha_B(2)|$. In a similar manner, larger $d_{B,\min}$ will be achieved by crafty design in the case of $|\alpha_B(1)| = |\alpha_B(2)|$. Consequently, larger $d_{i,\min}$, $i \in \{A, B\}$, will be achieved when $|\alpha_i(l)| = |\alpha_i(l')|$, where $l, l' \in \mathcal{N}$. In this scenario, the incremental bits of PS-NOMA come from Θ , which in turn reduces the design complexity of \mathbf{G} . Relevant content is also discussed in Section. IV. \square

IV. NUMERICAL RESULTS

In this section, we illustrate the BER and achievable rate performance of the proposed scheme through Monte Carlo simulation and numerical results. Since the power coefficients of PS-NOMA are randomly varying, from the fairness perspective, we set the counterpart without PS (denoted by NOMA) as a regular NOMA scheme. The average powers of h_A, h_B are set to be $\beta_A = 10, \beta_B = 1$, respectively. For brevity, we will refer to “PS-NOMA (M_A -PAM, M_B -PAM, N)” as the PS-NOMA scheme where the BS has N PLs and maps the information bits for U_A and U_B into M_A -PAM and M_B -PAM, respectively. Similarly, “NOMA (M_A -PAM, M_B -PAM)” denotes the NOMA scheme with M_A -PAM and M_B -PAM signals intended for U_A and U_B , respectively. Besides, we take $\text{SNR}=1/N_0$ as the horizontal axis of the following figures.

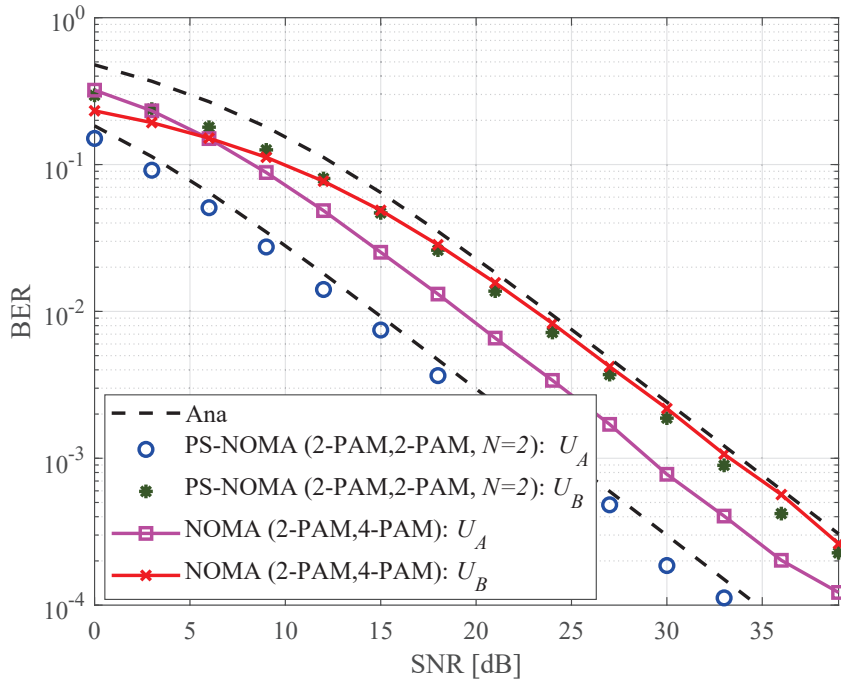


Fig. 6. BER comparison between PS-NOMA and NOMA.

A. BER Performance

In this subsection, the BER performance of PS-NOMA and NOMA is compared, assuming that U_A and U_B in all considered schemes employ ML detection. Since the comparison of OMA and NOMA has been widely argued in previous works, the BER curves of OMA counterparts are not presented.

In Fig. 6, we compare the BER performance of “PS-NOMA (2-PAM, 2-PAM, $N = 2$)” and “NOMA (2-PAM, 4-PAM)” with their theoretical BER results presented. Given fairness, we assume that the maximum spectral efficiency for both schemes are 3 bits per second per Hertz (bps/Hz), and both schemes have the same constellation order. According to **Lemma 1** and **Corollary 1**, the power matrices of “PS-NOMA (2-PAM, 2-PAM, $N = 2$)” and “NOMA (2-PAM, 4-PAM)” are set by

$$\mathbf{G} = \begin{bmatrix} \sqrt{0.2}, & \sqrt{0.8} \\ \sqrt{0.2} \exp(j\pi/2), & \sqrt{0.8} \exp(j\pi/2) \end{bmatrix} \quad (56)$$

and $\mathbf{G} = [\sqrt{0.2}, \sqrt{0.8}]$, respectively. It can be seen from Fig. 6 that the theoretical curves approximately match with their simulation counterparts. Besides, one can find that the BER performance of U_A is superior to that of U_B in both PS-NOMA and NOMA, which comes

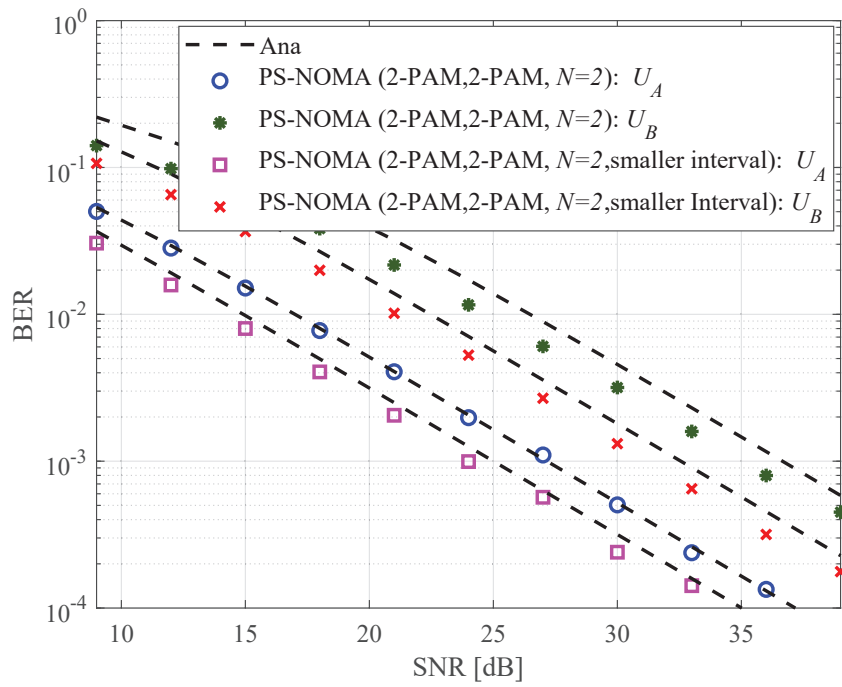


Fig. 7. BER comparison between PS-NOMA schemes with different PL intervals: Case 1.

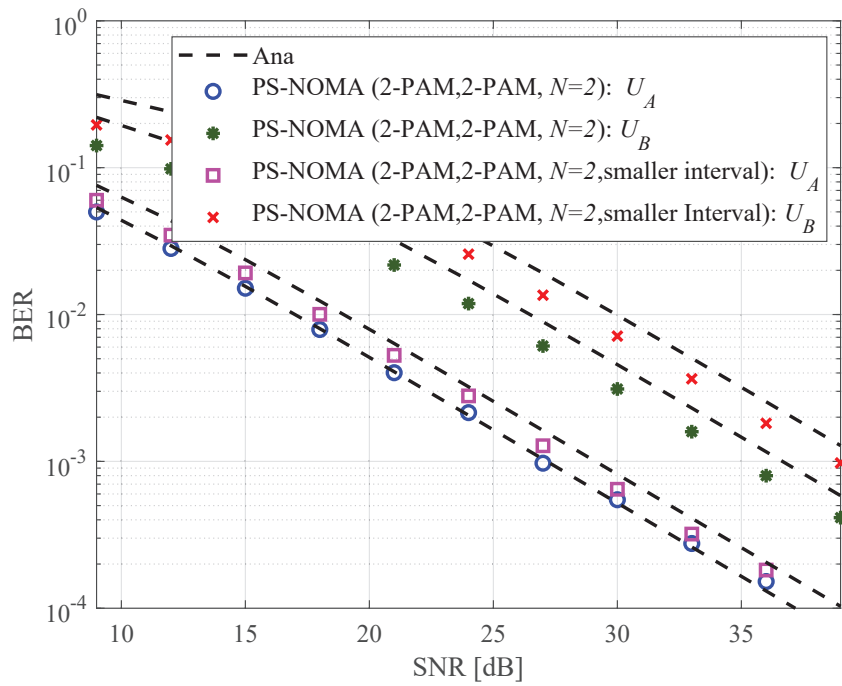


Fig. 8. BER comparison between PS-NOMA schemes with different PL intervals: Case 2.

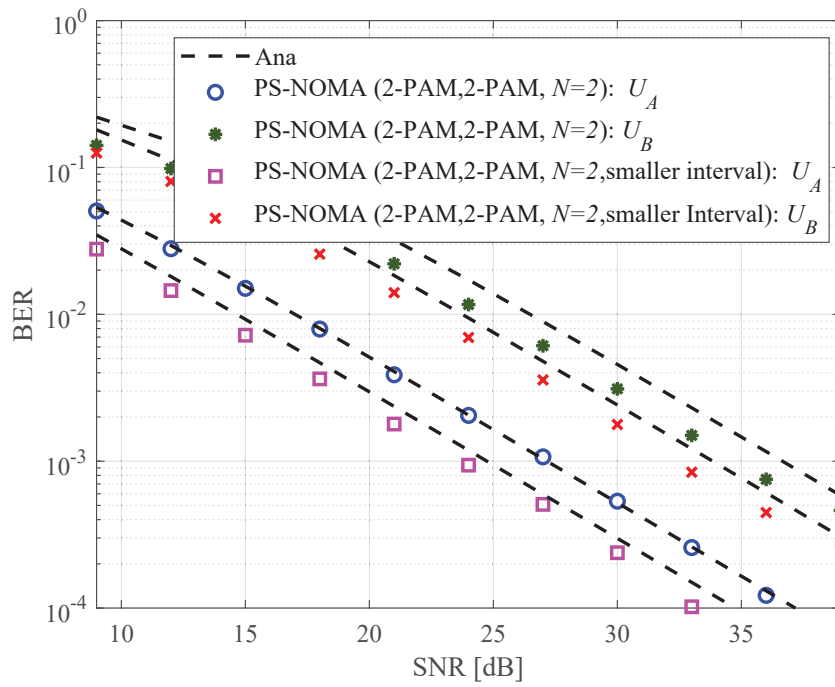


Fig. 9. BER comparison between PS-NOMA schemes with different PL intervals: Case 3.

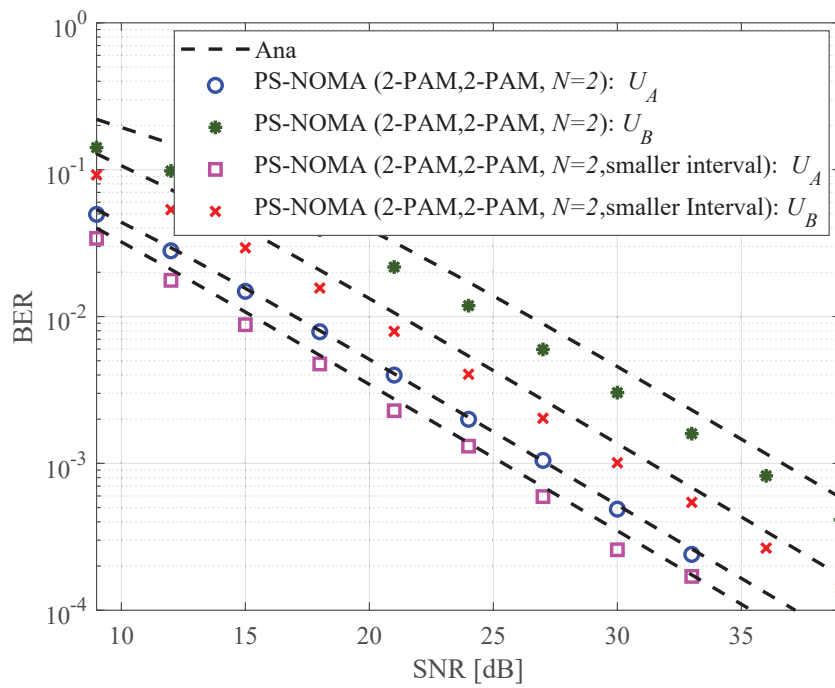


Fig. 10. BER comparison between PS-NOMA schemes with different PL intervals: Case 4.

from the fact $\beta_A > \beta_B$. Although all the curves have the same constellation order as 8, the performances of PS-NOMA are always better than those of NOMA. This phenomenon tells us that applying PS can improve performance without increasing constellation complexity when the amplitudes of power allocation coefficients of the system are the same.

Figure 7, 8, 9, and 10 respectively investigate four different scenarios where the power matrices of the compared counterparts

$$\mathbf{G} = \begin{bmatrix} \sqrt{0.1}, & \sqrt{0.9} \\ \sqrt{0.2} \exp(j\pi/2), & \sqrt{0.8} \exp(j\pi/2) \end{bmatrix} \quad (57)$$

for case 1,

$$\mathbf{G} = \begin{bmatrix} \sqrt{0.3}, & \sqrt{0.7} \\ \sqrt{0.4} \exp(j\pi/2), & \sqrt{0.6} \exp(j\pi/2) \end{bmatrix} \quad (58)$$

for case 2,

$$\mathbf{G} = \begin{bmatrix} \sqrt{0.2}, & \sqrt{0.8} \\ \sqrt{0.2} \exp(j\pi/2), & \sqrt{0.8} \exp(j\pi/2) \end{bmatrix} \quad (59)$$

for case 3, and

$$\mathbf{G} = \begin{bmatrix} \sqrt{0.1}, & \sqrt{0.9} \\ \sqrt{0.1} \exp(j\pi/2), & \sqrt{0.9} \exp(j\pi/2) \end{bmatrix} \quad (60)$$

for case 4, respectively. Besides, the power matrix of the benchmark, i.e., PS-NOMA (2-PAM, 2-PAM, $N = 2$), equals

$$\mathbf{G} = \begin{bmatrix} \sqrt{0.1}, & \sqrt{0.9} \\ \sqrt{0.4} \exp(j\pi/2), & \sqrt{0.6} \exp(j\pi/2) \end{bmatrix}. \quad (61)$$

Here the PL interval denotes the absolute difference between the absolute values of two adjacent rows of \mathbf{G} . Smaller interval denotes smaller value of PL interval than (61). Hence all the cases correspond to smaller intervals. We first discuss the BER performance of U_B . Concretely, in cases 1, 3, and 4, the minimum Euclidean distances of s_B are larger than those of the benchmark according to (52). Hence they show better BER performances, while opposite observations are found in the other cases. Furthermore, the phenomenon that performance of case 4 is better than that of benchmark also confirms the correctness of **Corollary 1**. More specifically, by comparing

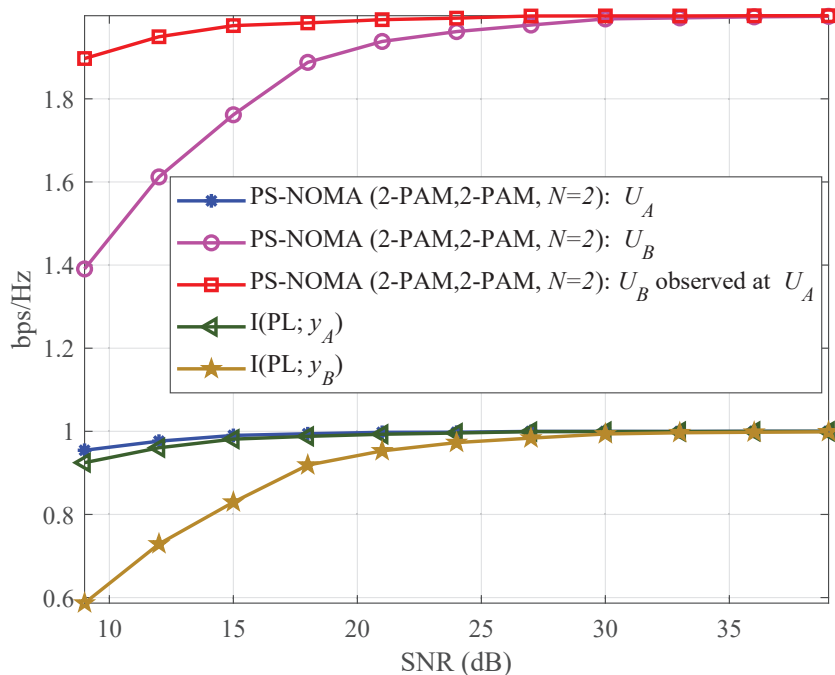


Fig. 11. Achievable rate and MI performance of PS-NOMA.

the curves of U_A in these cases, we observe that the minor power of U_A does not decrease the BER performance of U_A . From (9) and (10), we know that false detection of s_B and PL may result in the wrong s_B , or wrong PL, or wrong s_B and PL. The first detection process (9) is related to both s_B and PL, and it is directly related to the correctness of (10), so the power of U_B has a more significant influence than U_A . Notably, we assume that $M_A = M_B$ in this figure. Therefore this conclusion stands. In a word, we can consistently achieve better BER performance through designing power matrices with the same power value when $N = 2$ and the design of lower-order matrices are much simpler than higher-order ones.

B. Achievable Rate Performance

In this subsection, we first evaluate the achievable rate and MI performance of the proposed PS-NOMA, and then compare the achievable rate of PS-NOMA with the NOMA counterparts.

In Fig. 11, we show the achievable rate and MI performance of PS-NOMA with (56) and $\mathbf{G} = (\sqrt{0.2}, \sqrt{0.8})$, respectively. As seen from the figure, all the curves grow steadily as the SNR increases at low-to-medium SNR while achieving floors at high SNR. Obviously, the rates of U_A obtained from (25), U_B obtained from (13), and U_B observed at U_A obtained from (22) saturate to $\log_2(M_A)$, $\log_2(NM_B)$, and $\log_2(NM_B)$, respectively. On the other hand, the MI curves

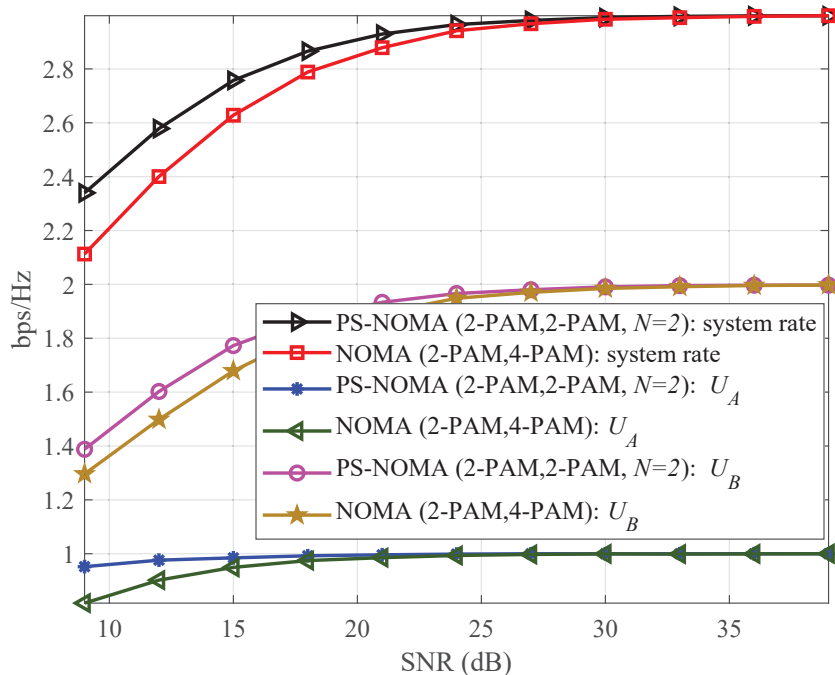


Fig. 12. Achievable rate comparison between PS-NOMA and NOMA.

$I(\text{PL}; y_A)$ and $I(\text{PL}; y_B)$ respectively denote the PL gains at U_A and U_B and are respectively generated from (24) and (21). Evidently, both curves saturate at 1 bps/Hz since the input entropy of the power-domain is $\log_2(N)$. In other words, all the gains gleaned from the power-domain are assigned to U_B . Moreover, since the channel quality of U_A is much better than that of U_B , the achievable rate or MI obtained at U_A is always higher than that at U_B , which guarantees the success of SIC.

Subsequently, in Fig. 12, we present the curves of PS-NOMA versus NOMA with the same system setups as Fig. 11. Compared to NOMA, PS-NOMA provides achievable rate gains for both U_A and U_B , and obtains the sum achievable rate enhancement in turn. This system performance improvement is more pronounced at low SNR, while the system gap narrows with increasing SNR. Since PS-NOMA and NOMA have the same constellation order, at high SNR, the achievable rate performances of them are equal. It is worth noting that the performance improvement of U_A is more obvious than that of U_B .

V. CONCLUSIONS

In this paper, we have proposed a novel two-user NOMA scheme using PS, in which the ordinary PAM symbol carries the bits of users. In addition, the BS randomly chooses a PL

from the power matrix preset for each transmission to carry more information. For PS-NOMA, approximate BER expressions have been derived in closed form for both users over Rayleigh flat fading channels. The rates and MI under finite input have also been developed. Computer simulations have verified the performance analysis and shown that the proposed scheme achieves better BER performance than conventional NOMA without increasing constellation complexity. Moreover, we observe that the proposed PS-NOMA can achieve better BER performance with the minimum number of PLs, which reduces the design difficulty of the power matrix. Furthermore, if we set an equal amplitude for each PL, the system performance will also increase. On the other hand, the proposed scheme also shows superior achievable rate performance compared to that of the NOMA counterpart. This work focuses only on the two-user scenario. We leave the more-user extension for future study.

APPENDIX A

PROOF OF (c)

To process step (c) of (26), we use the method introduced in [28]. Let $\mathcal{D} \triangleq -|h_B \Delta x_B|^2 - 2\mathcal{R}\{w_B^* h_B \Delta x_B\}$. With $w_B = h_B x_A + n_B$, \mathcal{D} can be rewritten as

$$\mathcal{D} = -|h_B \Delta x_B|^2 - |h_B|^2 2\mathcal{R}\{x_A^* \Delta x_B\} - 2\mathcal{R}\{n_B^* h_B \Delta x_B\}. \quad (\text{A.1})$$

Obviously, \mathcal{D} is Gaussian distributed with

$$\mathbb{E}\{\mathcal{D}\} = -|h_B \Delta x_B|^2 - |h_B|^2 2\mathcal{R}\{x_A^* \Delta x_B\} \quad (\text{A.2})$$

and

$$\text{Var}\{\mathcal{D}\} = \text{Var}\{n_B^* h_B \Delta x_B\} = 2N_0 |h_B \Delta x_B|^2. \quad (\text{A.3})$$

Therefore, we have $\Pr(\mathcal{D} > 0) = Q(-\mathbb{E}\{\mathcal{D}\}/\sqrt{\text{Var}\{\mathcal{D}\}})$, which can be easily simplified as the result of (c).

REFERENCES

- [1] Ericsson, “Cellular networks for massive IoT,” Tech. Rep. Uen 284 23-3278, Jan. 2016.
- [2] L. Dai, B. Wang, Y. Yuan, S. Han, C.-L. I, and Z. Wang, “Non-orthogonal multiple access for 5G: Solutions, challenges, opportunities, and future research trends,” *IEEE Commun. Mag.*, vol. 53, no. 9, pp. 74–81, Sep. 2015.
- [3] Y. Liu, Z. Ding, M. ElKashlan, and H. V. Poor, “Cooperative non-orthogonal multiple access with simultaneous wireless information and power transfer,” *IEEE J. Sel. Areas Commun.*, vol. 34, no. 4, pp. 938–953, Apr. 2016.
- [4] J. Liberti, S. Moshavi, and P. Zabolocky, “Successive interference cancellation,” U.S. Patent 8 670 418 B2, Mar. 2014.
- [5] M. Vaezi, Z. Ding, and H. V. Poor, *Multiple Access Techniques for 5G Wireless Networks and Beyond*. Springer International Publishing, 2019.
- [6] Z. Ding, Z. Yang, P. Fan, and H. V. Poor, “On the performance of non-orthogonal multiple access in 5G systems with randomly deployed users,” *IEEE Signal Process. Lett.*, vol. 21, no. 12, pp. 1501–1505, Dec. 2014.
- [7] Z. Ding, Y. Liu, J. Choi, Q. Sun, M. ElKashlan, I. Chih-Lin, and H. V. Poor, “Application of non-orthogonal multiple access in LTE and 5G networks,” *IEEE Commun. Mag.*, vol. 55, no. 2, pp. 185–191, Feb. 2017.
- [8] S. M. R. Islam, N. Avazov, O. A. Dobre, and K. Kwak, “Power-domain non-orthogonal multiple access (NOMA) in 5G systems: Potentials and challenges,” *IEEE Commun. Surveys Tuts.*, vol. 19, no. 2, pp. 721–742, Secondquarter 2017.
- [9] “3rd generation partnership project; technical specification group radio access network; study on non-orthogonal multiple access (NOMA) for NR, release 16, (V16.0.0),” 3GPP, Sophia Antipolis, France, Rep. TR 38.812, Dec. 2018.
- [10] D. Slepian and J. K. Wolf, “A coding theorem for multiple access channels with correlated sources,” *Bell Syst. Tech. J.*, vol. 52, no. 7, pp. 1037–1076, 1973.
- [11] R. S. Cheng and S. Verdú, “Gaussian multiaccess channels with ISI: Capacity region and multiuser water-filling,” *IEEE Trans. Inf. Theory*, vol. 39, no. 3, pp. 773–785, May 1993.
- [12] G. Caire and S. Shamai (Shitz), “On the achievable throughput of a multi-antenna Gaussian broadcast channel,” *IEEE Trans. Inf. Theory*, vol. 49, no. 7, pp. 1691–1706, Jul. 2003.
- [13] T. M. Cover and J. A. Thomas, *Elements of Information Theory*, 2nd ed. Hoboken, NJ, USA: Wiley, 2006.
- [14] A. Lozano, A. M. Tulino, and S. Verdú, “Optimum power allocation for parallel Gaussian channels with arbitrary input distributions,” *IEEE Trans. Inf. Theory*, vol. 52, no. 7, pp. 3033–3051, Jul. 2006.
- [15] J. Harshan and B. S. Rajan, “On two-user Gaussian multiple access channels with finite input constellations,” *IEEE Trans. Inf. Theory*, vol. 57, no. 3, pp. 1299–1327, Mar. 2011.
- [16] J. Harshan and B. S. Rajan, “A novel power allocation scheme for two-user GMAC with finite input constellations,” *IEEE Trans. Wireless Commun.*, vol. 12, no. 2, pp. 818–827, Feb. 2013.
- [17] Z. Dong, H. Chen, J. Zhang, and L. Huang, “On non-orthogonal multiple access with finite-alphabet inputs in Z-channels,” *IEEE J. Sel. Areas Commun.*, vol. 35, no. 12, pp. 2829–2845, Dec. 2017.
- [18] Z. Dong, H. Chen, J. Zhang, L. Huang, and B. Vucetic, “Uplink non-orthogonal multiple access with finite-alphabet inputs,” *IEEE Trans. Wireless Commun.*, vol. 17, no. 9, pp. 5743–5758, Sept. 2018.
- [19] Y. Yang and B. Jiao, “Information-guided channel-hopping for high data rate wireless communication,” *IEEE Commun. Lett.*, vol. 12, no. 4, pp. 225–227, Apr. 2008.
- [20] C. Liu, M. Ma, Y. Yang, and B. Jiao, “Optimal spatial-domain design for spatial modulation capacity maximization,” *IEEE Commun. Lett.*, vol. 20, no. 6, pp. 1092–1095, Jun. 2016.
- [21] Y. Chen, L. Wang, Y. Ai, B. Jiao, and L. Hanzo, “Performance analysis of NOMA-SM in vehicle-to-vehicle massive MIMO channels,” *IEEE J. Sel. Areas Commun.*, vol. 35, no. 12, pp. 2653–2666, Dec. 2017.

- [22] Q. Li, M. Wen, E. Basar, H. V. Poor, and F. Chen, "Spatial modulation-aided cooperative NOMA: Performance analysis and comparative study," *IEEE J. Sel. Topics Signal Process.*, vol. 13, no. 3, pp. 715–728, Jun. 2019.
- [23] X. Wang, J. Wang, L. He, Z. Tang, and J. Song, "On the achievable spectral efficiency of spatial modulation aided downlink non-orthogonal multiple access," *IEEE Commun. Lett.*, vol. 21, no. 9, pp. 1937–1940, Sept. 2017.
- [24] X. Wang, J. Wang, L. He, and J. Song, "Spectral efficiency analysis for downlink NOMA aided spatial modulation with finite alphabet inputs," *IEEE Trans. Veh. Technol.*, vol. 66, no. 11, pp. 10562–10566, Nov. 2017.
- [25] L. Pan and J. Zheng, "Spatial modulation aided cooperative NOMA: Implementation and achievable rate analysis," in *Proc. IEEE Int. Conf. Commun. (ICC)*, Shanghai, China, May 2019, pp. 1–6.
- [26] Y. -Y. Zhang and J. -K. Zhang, "Fundamental applicability of spatial modulation: High-SNR limitation and low-SNR advantage," *IEEE J. Sel. Areas Commun.*, vol. 37, no. 9, pp. 2165–2178, Sept. 2019.
- [27] L. Bariah, A. Al-Dweik, and S. Muhaidat, "On the performance of Non-orthogonal multiple access systems with imperfect successive interference cancellation," in *Proc. IEEE Int. Conf. Commun. (ICC)*, Kansas City, MO, USA, May 2018, pp. 1–6.
- [28] E. Başar, Ü. Aygözü, E. Panayırıcı, and H. V. Poor, "Orthogonal frequency division multiplexing with index modulation," *IEEE Trans. Signal Process.*, vol. 61, no. 22, pp. 5536–5549, Nov. 15, 2013.
- [29] M.-S. Alouini and A. J. Goldsmith, "A unified approach for calculating error rates of linearly modulated signals over generalized fading channels," *IEEE Trans. Commun.*, vol. 47, no. 9, pp. 1324–1334, Sept. 1999.
- [30] K. Cho and D. Yoon, "On the general BER expression of one-and two dimensional amplitude modulations," *IEEE Trans. Commun.*, vol. 50, no. 7, pp. 1074–1080, Jul. 2002.